Digital Discovery

ROYAL SOCIETY OF CHEMISTRY

PAPER

Published on 16 September 2026
Licensed under CC-BY-NC 4.0

Check for updates

Cite this: DOI: 10.1039/d6dd00402d

Breaking the digital-physical barrier in organic electronics materials discovery: application to finding anti-Kasha molecules

Ömer H. Omar,*[a] Daniele Padula,[b] Kate A. Morrison,[a] Krzysztof Pawlak,[a] Alexander Ciupa,[a] Dávid Havasi[cd] and Alessandro Troisi*[a]

Received 21st June 2026
Accepted 3rd September 2026

DOI: 10.1039/d6dd00402d

rsc.li/digitaldiscovery

Molecules which display two optical emission bands are very rare as they violate Kasha's rule, which states that fluorescence is normally observed only from the lowest energy excited state of a specific spin multiplicity (*e.g.* S_1) due to efficient internal conversion from higher states after excitation. Here, we develop a combined virtual and experimental screening workflow to find new anti-Kasha emitters among those with a large energy gap between S_1 and S_2; a condition that favours optical emission from the higher excited state because of a reduced internal conversion rate. 140 000 chemically diverse and commercially available molecules are filtered through a computational funnel based on their computed S_1–S_2 gap, transition intensities and structural rigidity before being ranked by cost and purity from up-to-date information from the chemical supply chain. The absorption and fluorescence spectra have been measured for 15 potential candidates that have not been previously explored for this property. Seven of them display anti-Kasha emission, five displaying single emission from S_2 and two displaying emission from multiple excited states (a particular case of dual emission). The lower energy emission of one of the dual emitters, however, originates from an aggregate state. The approach exemplifies the great potential of virtual screening approaches that take into account chemical availability and lead to an immediate validation of the predictions.

1. Introduction

Digital discovery tools are now regularly used in virtually all areas of chemistry,[1,2] including all branches of organic electronics.[3,4] The discovery of molecules with desirable optical and electronic properties is particularly suitable for high-throughput virtual screening (HTVS) studies and many have appeared in the past few years identifying candidates with properties such as thermally activated delayed fluorescence,[5] singlet fission,[6] or high charge mobility.[7] Several HTVS campaigns constructed to explore well-known design principles (*e.g.* donor–acceptor molecules for TADF) have been proven successful when the predictions were tested experimentally[8,9] especially in highly-automatised labs.[10,11] Much more challenging is the experimental testing of HTVSs that explore a broader chemical space, looking for novel molecular architectures and design principles.[12,13] The candidates found in this way, also if already known to chemistry, tend to be characterised by highly diverse synthetic pathways requiring considerable labour and specialisation to be synthesised and tested. The barrier between digital discovery and testing can be completely removed if the availability for immediate experimental testing is used to identify the molecules to be screened in the first place. The objective of this work is to illustrate how molecules sampled from virtually the entire chemical supply chain can be screened for interesting electronic properties and then readily tested.

In this work we consider searching for molecules displaying anti-Kasha emission, *i.e.* emission from higher excited states, and dual emission produced by prompt emission from multiple excited states. Such properties can be readily verified in the lab, where the latter is sought after for applications in sensing,[14,15] imaging,[16] displays[17] and optical storage.[18] The vast majority of emissive molecules follows Kasha's rule,[19] *i.e.* the emitting electronic level of a given multiplicity is the lowest excited state of that multiplicity. For neutral closed-shell molecules, for which phosphorescence can be ruled out, such as molecules in liquid solution, the rule implies that one should observe only emission from the lowest singlet excited state (S_1). Higher excited states relax rapidly toward this lowest excited state through internal conversion, a process faster between energetically closer states (energy gap law[20,21]) while there is normally

[a]*Department of Chemistry, University of Liverpool, Liverpool, L69 3BX, UK. E-mail: omer@apoello.com; a.troisi@liverpool.ac.uk*

[b]*Dipartimento di Biotecnologie, Chimica e Farmacia, Università di Siena, Via A. Moro 2, I-53100 Siena, Italy*

[c]*Mcule.com Kft, Bartók Béla út 105-113, Budapest, 1115, Hungary*

[d]*Department of Chemical and Environmental Process Engineering, Budapest University of Technology and Economics, Műegyetem Rakpart 3, Budapest, 1111, Hungary*

© 2026 The Author(s). Published by the Royal Society of Chemistry

a much larger gap between S_1 and the ground state, S_0. Emission from S_2 can be observed when there is a large energy gap between S_2 and S_1,[22,23] with azulene[24,25] being an archetypal example, however with virtually all of the emission from S_2. HTVS is the ideal approach to find completely new molecules with unusually large gaps between S_2 and S_1, since there is no simple chemical intuition for these properties other than modifying known motifs.[26,27] This approach, however, would not capture molecules displaying dual emission *via* alternative mechanisms[28–33] such as repopulation of the S_2 state,[22] excited-state intramolecular proton transfer (ESIPT),[34] triplet-detouring,[22] temperature-activated delayed fluorescence[35] and aggregation-induced emission.[36] An additional complication for the screening perspective is that the observation of non-Kasha emission can be due to artifacts as noted for example in ref. 37, which need to be excluded.

We present in the Methods section the virtual screening protocol we have constructed with its assumption, while the Results section discusses the key findings from the virtual screening and their experimental verification. The Conclusions propose possible improvement in the development of mixed computational and experimental workflows for molecules with interesting photophysical properties.

2. Methods

The full library of molecules considered initially was the subset of 12 million molecules from the ZINC database (2019),[38] originally developed for medicinal chemistry applications, collecting all molecules that have been commercially available and labelled as "in-stock" according to the supplier. To find organic molecules with interesting electronic properties (orbital and excited state energies) it is extremely convenient to sample from such a large database only molecules that have different conjugated cores, defined as the largest portion of the molecule with a continuous connection of sp^2-hybridised atoms. Molecules with the same conjugated core are expected to have similar electronic properties, an approximation validated below. The first step of the screening is therefore to cluster the initial set of 12 million molecules into sets that share the same conjugated core (see SI for further details). The dataset contains over 140 000 structures with a distinct conjugated core and the smallest molecule of each cluster is chosen as a representative of the electronic properties for that conjugated-core set. This reduces the computational cost by over a factor of 80, whilst still describing the larger set with an easily controlled approximation. In the SI, we show using a randomised small sample that 67% of the molecules have S_1 excitation energies within 0.1 eV (87% within 0.3 eV) of their conjugated-core analogue, and 69% have S_2 excitation energies within 0.1 eV (89% within 0.3 eV) of their conjugated-core analogue. Clearly, having identified a representative molecule with interesting electronic properties, the method gives immediate access to all its analogues for further consideration. The computational procedure, detailed in the SI and validated against experimental data, involves the generation of 3D molecular coordinates from the SMILES (a character string representation of the molecule[39]), conformational search using the Universal Force Field[40] implemented in RDKit,[41] DFT optimisation at the BLYP35/3-21G* level and TD-DFT calculations of excited states at the M06-2X/3-21G* level. The energy gaps are computed in the geometry of the ground state as well as the intensity of the transitions, quantified from the oscillator strength. In the SI it is shown that the procedure offers a good balance between accuracy and speed of execution.

A prerequisite for this approach to be valid is to verify that the energy gap allows identification of molecules with potential anti-Kasha emission. Fig. 1 shows the distribution of the ratio between the S_1–S_2 energy gap $E(S_2)$–$E(S_1)$ and the excitation energy of S_1, $E(S_1)$–$E(S_0)$ for the 107 000 molecules out of the 140 000 distinct conjugated cores with oscillator strength for both the first ($f(S_1)$) and second ($f(S_2)$) excited state larger than 0.0001. The median of this parameter is 0.07, *i.e.* the S_2–S_1 gap is typically much smaller than the S_1–S_0 gap with only 2% of the molecules displaying $[E(S_2)–E(S_1)]/[E(S_1)–E(S_0)] \geq 0.4$. The figure also reports the range of this parameter for ∼20 experimentally known anti-Kasha emitters (dual emission or emission from S_2), which are explicitly listed in Table S2 of the SI. Clearly these emitters have a much larger $[E(S_2)–E(S_1)]/[E(S_1)–E(S_0)]$ with a median value of 0.45, and one can immediately see that the greatest chance of success in finding anti-Kasha emitters is in the scarcely populated region with large $[E(S_2)–E(S_1)]/[E(S_1)–E(S_0)]$. This descriptor is directly linked with the original physical justification of Kasha's rule. Internal conversion rate decreases exponentially with the increase of the energy gap between initial and final state (Energy Gap law). Since the $E(S_2)$–$E(S_1)$ gap (and all $E(S_{n+1})$–$E(S_n)$ gaps for $n > 1$) is typically much smaller than the $E(S_1)$–$E(S_0)$ gap, the population rapidly relax non-radiatively to S_1 before emitting from other excited states. Exception to Kasha's rule are therefore expected for $E(S_2)$–$E(S_1)$ becoming comparable to $E(S_1)$–$E(S_0)$.

The oscillator strengths could also be expected to be important for anti-Kasha emission; for example, a strong $f(S_2)$ could accelerate direct emission from S_2 against the competing internal conversion. However, the median computed oscillator

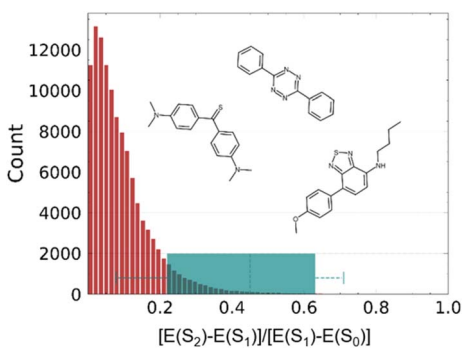


Fig. 1 Distribution of $[E(S_2)–E(S_1)]/[E(S_1)–E(S_0)]$. The overlayed boxplot shows how the known anti-Kasha emitters are distributed within the larger distribution. They are listed in Table S2 and depicted in Fig. S7 of the SI. The chemical structures of three known anti-Kasha emitters are also displayed as examples. Molecules with vanishing oscillator strengths have been removed.

© 2026 The Author(s). Published by the Royal Society of Chemistry

strength of the known anti-Kasha emitters is similar to the rest of the dataset (0.017 and 0.005 for $f(S_1)$ and $f(S_2)$ respectively), meaning that we are unable to downselect candidates on the basis of oscillator strengths. We have therefore simply imposed a minimum threshold to both to exclude molecules with dark states. So far, only the vertical $S_0 \rightarrow S_n$ ($n = 1, 2$) transition energies have been considered; however, for emission excited-state minima can be considered for better accuracy. This can be best achieved by optimising excited states, which is too computationally expensive in a screening setting; therefore, we opt to continue using the vertical $S_0 \rightarrow S_n$ transition energies which will be then compared more directly with experimental absorption energies.

We did not include the effect of the solvent because the solvent to be used was not known in the virtual screening phase. Its inclusion can be important to improve theory-experiment comparison and could be used in virtual screening method[42] but, given the small number of candidates and the uncertainty on their solubility, we opted for a direct experimental evaluation of the solvent effect. Similarly, given the small number of candidates to be evaluated experimentally it was deemed unnecessary to perform further calculations (*e.g.* of excited state optimization).

3. Results and discussion

The overall HTVS protocol is illustrated in Fig. 2. After the first screening of only molecules with a distinct conjugated core, we have considered further those 2821 entries with $[E(S_2)–E(S_1)]/[E(S_1)–E(S_0)] \geq 0.4$. This limit is chosen to give additional confidence to the candidates, *i.e.* the larger the ratio, the better, while still sampling a large number of compounds. An oscillator strength condition of min $(f(S_1), f(S_2)) > 0.009$ is applied, giving 200 compounds, all expected to be emissive. We then filter the candidates further based on rigidity by considering only those with a number of rotatable bonds, $n_{rots} \leq 4$ (n_{rots} is computed as implemented in RDKit[41]). This condition should reduce the chance of non-radiative decay through conical intersections[43] which are prevalent in flexible molecules;[44] this yields 145 structures. Since availability of specialty chemicals, delivery time and cost are highly dynamic, we checked for current commercial availability and produced a cost-ranked list of 78 promising unique-core candidates for experimental testing. These are reported in the SI for verification and possible testing by interested readers. It should be noted that analogues of experimentally known anti-Kasha emitters are also present within this set, such as azulene, which serves as a quick verification of the protocol's capacity to identify useful materials. After (i) setting a cost limit of \$50/mg^{-1}, (ii) ensuring that at least 1 mg of each compound was available with (iii) guaranteed purity >90% and (iv) delivery time was less than 4 weeks, we select 19 compounds from this collection for experimental testing; these are illustrated in Fig. 3. The computational cost of the entire procedure can be estimated as 250 000 CPU hours. However, it should be noted that results can be reused to screen for different properties[45] or to validate approximated computational methods.[46,47]

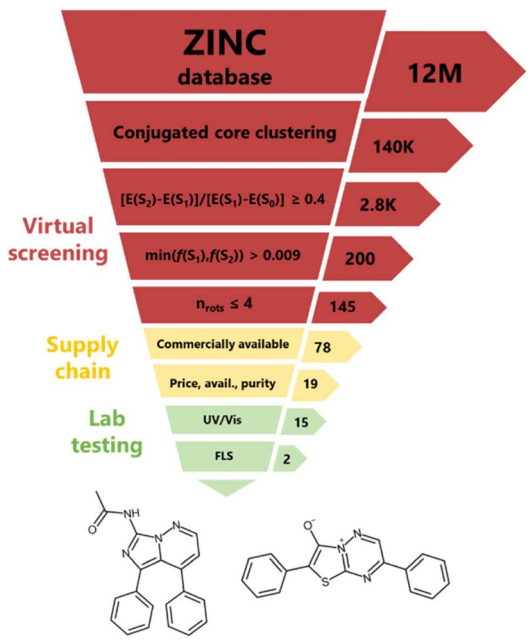


Fig. 2 The expanded screening funnel workflow, where the dataset size after each stage is given in the tabs on the right, showing a gradual decrease from a set of over 12 million into the final candidates (depicted below).

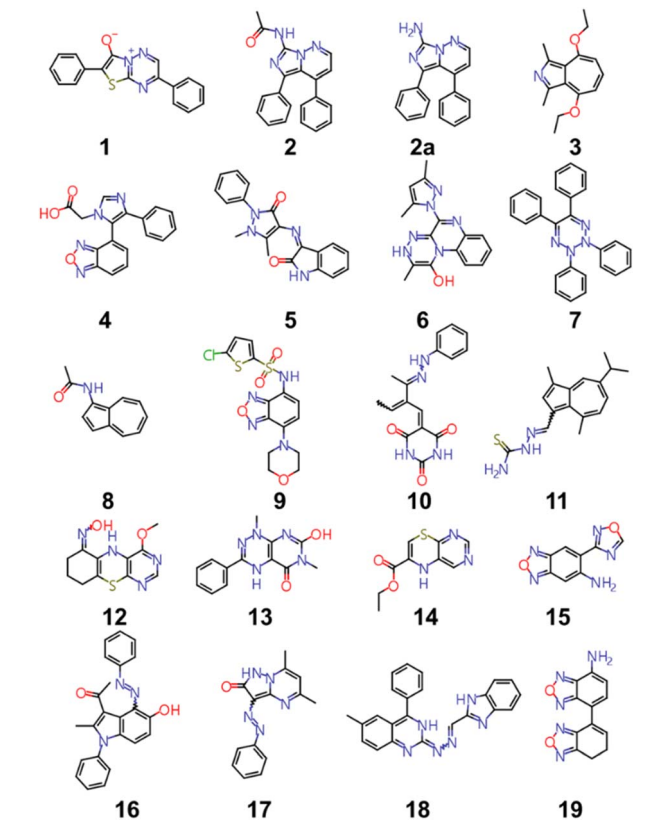


Fig. 3 Chemical structures of experimentally-tested candidates.

© 2026 The Author(s). Published by the Royal Society of Chemistry

All quoted with > 90% purity, the compounds are first measured using UV/vis absorption spectroscopy to confirm whether a molecule can be expected to be anti-Kasha emitters on the basis of a large experimental $[E(S_2)–E(S_1)]/[E(S_1)–E(S_0)]$ (see Table S3). 15 out of 19 molecules display experimental $[E(S_2)–E(S_1)]/[E(S_1)–E(S_0)] > 0.2$ and are therefore considered further with fluorescence spectroscopy. All spectra are reported in the SI and, since the goal is to identify rapidly new anti-Kasha emitters, molecules with inconclusive spectra are not considered further. The molecules for which spectra were measured are divided into (i) molecules displaying the sought-after dual emission in this preliminary exploration stage (**1**, **2** (**2a**), which are illustrated in Fig. 4 and discussed further below); (ii) molecules displaying unusual (but technologically less relevant) anti-Kasha emission from S_2 (**3**, **4**, **5**, **6** and **7**, illustrated in Fig. S9); (iii) molecules displaying conventional single emission from S_1 (**8**, **9**, **10**, **11**, **12** and **13**, illustrated in Fig. S10); and (iv) the SI also reports, for completeness, the inconclusive spectra of **14**, **15**, **16**, **17**, **18** and **19** in Fig. S11. This latter group could not be assigned to groups (i)–(iii) because of low emission intensity under measured condition, low solubility in the two solvents considered (DMSO and methanol). The following discussion focuses on those materials deemed to be dual emitters.

Compound **1** (2,7-diphenyl-4lambda5-[1,3]thiazolo[3,2-*b*][1,2,4]triazin-4-ylium-3-olate) is, to the best of our knowledge, not known as a material for electronics applications. Its analogues are used as therapeutic agents in the treatment of anti-inflammatory rheumatic diseases.[48] Increasing the level of theory (see SI) for higher fidelity when comparing to experiment, the computed wavelengths for the $S_0 \rightarrow S_1$, $S_0 \rightarrow S_2$ and $S_0 \rightarrow S_3$ transitions are 597 nm, 416 nm and 333 nm which are in excellent agreement with the experimental absorption peak positions in Fig. 4a. The computed energies for the $S_1 \rightarrow S_0$ and $S_2 \rightarrow S_0$ emission transitions, *i.e.* using the geometry of the corresponding excited state minima, are 703 nm and 510 nm respectively. For the $S_1 \rightarrow S_0$ emission, the strong near-infrared peak at 786 nm can be assigned, yielding a Stokes shift of nearly half an electron-volt for the transition. Any potential $S_3 \rightarrow S_1$ transition is computed at 1077 nm and can be ruled out. The large, second experimental emission peak at 358 nm does not correspond to the computed $S_2 \rightarrow S_0$ emission but matches more closely the $S_3 \rightarrow S_0$ emission peak computed at 380 nm. The higher-energy peak itself is not smooth and the hump at approximately 450 nm could be the $S_2 \rightarrow S_0$ present underneath, thus the possibility of prompt triple emission cannot be ruled out. To rule out the possibility of a protonated species, the electronic energy requirement for protonation in methanol is computed (see detail in SI) and predicted to be +188 $kJmol^{-1}$, making it significantly unfavourable. To ensure there was no effect of contaminants and for further characterisation, we

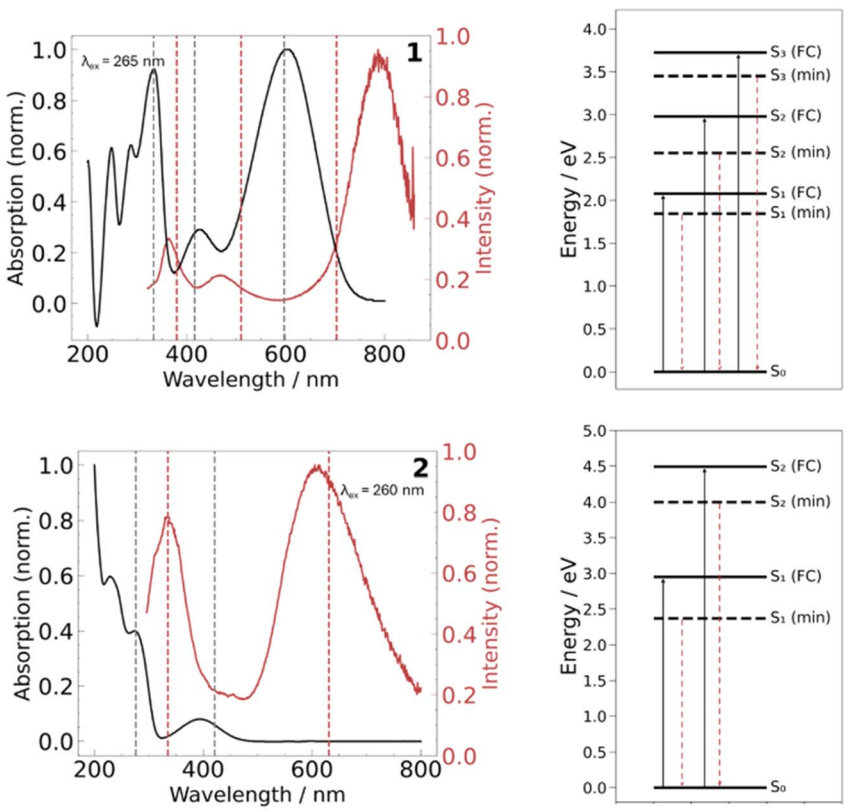


Fig. 4 Absorption (black) and emission (red) spectra of compounds **1** and **2** measured in methanol. Black dashed lines indicate computed vertical absorption energies. Red dashed lines indicate computed vertical emission energies. Electronic states of interest are given on the panel on the right for each spectrum; min = minimum, FC = Franck–Condon transition at S_0 geometry; black solid arrows are absorption transitions, red dashed lines are emission transitions.

© 2026 The Author(s). Published by the Royal Society of Chemistry

repurchased compound **1**, remeasured it and confirmed its purity and chemical identity *via* LC-MS as shown in Fig. S12, making the discovery more robust and ruling out the presence of alternative species coexisting in solution. Experimental variations in the spectra of this sample based on excitation wavelength and concentrations are further detailed in the SI to help rule out additional effects such as aggregation (see Fig. S13, also excluding the effect of protonation).

Compound **2** (*N*-{4,5-diphenylimidazo[1,5-*b*]pyridazin-7-yl} acetamide) has no active patent, nor is it directly considered in any electronics applications. Its core structure imidazo[1,5-*b*] pyridazine is, however, known for medicinal applications.[49] It shares some similarity, *i.e.* nitrogen-substituted analogue, with the imidazo[1,2-*b*]pyridazine core which has recently been discovered for use in high-performance red-phosphorescent OLEDs.[50] The core structure also shares similarity with pyrazolo[1,5-*a*]pyrimidine, whereby some of its derivatives have been suggested as highly tuneable and sustainable fluorophores.[51] The (high-level) computed wavelengths for the $S_0 \rightarrow S_1$ and $S_0 \rightarrow S_2$ transitions are 421 nm and 276 nm, respectively, and match the experimental absorption peaks in Fig. 4. The computed vertical emission energies for the $S_1 \rightarrow S_0$ and $S_2 \rightarrow S_0$ transitions (using the geometry of the corresponding excited state minima) are 641 nm and 335 nm, corresponding closely to the experimental photoluminescence maxima at 605 nm and 336 nm. This results in a Stokes shift exceeding 1 eV for the S_1 state, in excellent agreement with the computed (gas-phase) Stokes shift of 1.01 eV, which is further analysed in the SI. We could not purchase compound **2** which became commercially unavailable during the course of the project (breaking the barrier between digital and physical discovery in HTVS requires consideration of the dynamic and volatile nature of the global chemical supply chain). Instead, we purchased a core analogue where the amide functional group is swapped for a primary amine (compound **2a**) and satisfied all theoretical conditions for dual emission as described above. The absorption spectrum of **2a** matches very strongly that of compound **2** and the emission spectrum still displays dual emission when measured in methanol (see Fig. S16), suggesting successful dual emission for this overall core. By directly comparing an amide (**2**) and amine (**2a**) analogue, it means that we do not expect any influence by tautomers or alternative species (*e.g.* protonated). In line with this hypothesis, the protonation energy of the most basic site of **2a** is computed to be +180 kJ mol^{-1}. However, there is a decrease in the intensity of the high-energy peak, which is also impacted when measured in acetonitrile, suggesting a potential for strong solvent interactions or aggregation.

The final set of measurements to confirm the presence of dual emission was performed on a newly purchased batch of molecule **1** and **2a** and included the study of absorption and emission at different concentration and the measurement of excitation spectra (also at different concentrations). The emission spectra of **1** do not show any dependence on the concentration and their excitation spectra are very similar to the absorption spectra (see Fig. S12). On the other hand, the emission intensity of the lower energy emission of **2a** decreases with decreasing concentration (Fig. S15) and the excitation spectrum does not match the absorption spectrum (Fig. S14). This observation, together with the disappearance of the low energy emission in acetonitrile (Fig. S16), suggests that the low energy emission of **2a** derives from an aggregate (high purity and chemical identity of **2a** is confirmed *via* LC-MS and given in Fig. S18). In this case, the existence of well-separated excited states is likely to contribute to the dual fluorescence, but other mechanistic effects such as the reduction of the non-radiative relaxation following aggregation may be at play.

It is worth considering the clear distinction between observing dual emission or emission from higher excited states (an experimental observation) and establishing the mechanism of anti-Kasha emission (a mechanistic conclusion). A conventional photochemistry work is concerned with elucidation of a mechanism for a restricted number of molecules. In a virtual screening approach, we often search for molecules for which a certain mechanism can be present and we impose enough constraints to the search to make such mechanism highly likely (energy gap, rigidity, oscillator strength). The assignment of a mechanism is built in the virtual search. As we have seen however for molecule **2a** and often found in literature,[52] the photophysics can be more complex than the one originally hypothesized. One can therefore conceive an additional investigation layer in the scheme of Fig. 2, where in-depth studies are performed on the interesting molecule. As we have seen, virtual screening is undoubtedly able to identify such interesting cases. Attempts to incorporate photophysical calculations directly into the virtual screening are ongoing,[53] but only a few tens of molecule can be computed in reasonable time with state of the art methods,[25,53] which also suffer from lower accuracy for non-radiative transitions with large energy gaps.[54]

4. Conclusions

Overall, we have devised an approach to screen all chemicals rapidly available *via* the chemical supply chain for optical and electronic properties, and illustrate the power of such a screening by identifying 145 potential dual emitters and, among them, 19 low-cost candidates. Through experimental characterisation, we have identified two apparent dual emitters and five anti-Kasha S_2 emitters, which is significant given the rarity of the phenomenon. Further investigation reveals that one of the molecules with apparent dual emission displays a low energy fluorescence signal that originates from an aggregate and disappears at low concentration (it remains an anti-Kasha emitter). The digital discovery process that is usually visualized as a funnel with increasingly stringent criteria and/or more accurate calculation contains a blend of cheminformatics queries, computational chemistry, further chemical supply chain information about cost and availability and a sequence of increasingly more complex measurements from simple UV/Vis absorption to multiple excitation and emission spectra. While our research is concluded at this stage, we envision additional levels of characterization (*e.g.* lifetime measurement or transient absorption spectroscopy) and additional synthetic work (the molecules identified can be seen as lead compounds for

© 2026 The Author(s). Published by the Royal Society of Chemistry

further optimization). Digital discovery can be seen just as the beginning of the discovery process.

Finally, it is worth noticing how the search from the space of commercially available molecules makes the process quite accessible and efficient and it can be easily expanded to cover virtual libraries, *i.e.* libraries of compounds that can be easily synthesised.

Conflicts of interest

This work was supported by the European Innovation Council (EIC) Transition program (No. 101057564). Mcule participated as a project partner; materials were purchased *via* their platform at standard commercial rates.

Data availability

All data required to reproduce and verify the results are given as part of the supplementary information (SI). Supplementary information: (i) the method for the computational chemistry calculation is given in section 5. (ii) The method to generate the initial geometry from the SMILES is given Section 3b. (iii) The list of known dual emitters are given as images in Fig. S7 and link to the original reference and key computational result in Table S2. (iv) The full IUPAC name, chemical supplier and computational results is given in Table 3. (v) All experimental spectra relevant for the discussion have been included in the SI (section 5). (vi) All commercially available candidates identified by the procedure (also if not considered experimentally) are listed in Section S2. (vii) (Minor) usage of other software such a Openbabel and RDKit. (viii) Algorithm for the definition of the conjugated core. (ix) Method to perform the clustering See DOI: https://doi.org/10.1039/d6dd00402d.

Acknowledgements

Ö. H. O and A. T. acknowledge funding from Horizon Europe (European Innovation Council, project no. 101057564). Ö. H. O and A. T. would like to acknowledge the assistance provided by Research IT and the use of the Barkla High Performance Computing facilities at the University of Liverpool. D. P. gratefully acknowledges funding from the Italian Ministry of University and Research (MUR, PRIN grant 2022CXHY3A) and from Programma CN00000013 of ICSC – Centro Nazionale di Ricerca in High Performance Computing, Big Data and Quantum Computing, funded by European Union – NextGenerationEU – PNRR, Missione 4 Componente 2 Investimento 1.4, SPOKE 7 Materials & Molecular Sciences, CUP B93C22000620006. The authors are grateful to Professor Stephen Meech for fruitful discussions and suggestions.

References

1 C. Li, J. Ma, D. Gibson, Y. Yan, M. Haroon and M. Bi Bi, Enhancing Energy Materials with Data-Driven Methods: A Roadmap to Long-Term Hydrogen Energy Sustainability Using Machine Learning, *Int. J. Hydrogen Energy*, 2025, **119**, 108–125, DOI: 10.1016/j.ijhydene.2025.03.201.

2 S. H. M. Mehr, Digital Discovery and the New Experimental Frontier, *Digital Discovery*, 2025, **4**(4), 892–895, DOI: 10.1039/D5DD00029G.

3 S. Shahzadi, T. Shahzadi, Z. Shafiq and M. R. S. A. Janjua, A Review on Fabrication and Quantum Chemical Designing of Organic Solar Cells: Role of DFT and Machine Learning Technologies, *High Energy Chem.*, 2024, **58**(6), 583–603, DOI: 10.1134/S0018143924700644.

4 L. Cui, Q. Li, Y. Zhang, J. Zhang, Z. Wang, J. Chen and B. Zheng, Machine Learning-Assisted High-Throughput Screening of Transparent Organic Light-Emitting Diode Anode Materials, *Chem. Sci.*, 2024, **15**(46), 19375–19389, DOI: 10.1039/D4SC05598E.

5 K. Thapa, J. I. Jones and L. E. Ratcliff, A High Throughput Virtual Screening Approach for Identifying New Thermally Activated Delayed Fluorescence-Based Emitters, *J. Mater. Chem. C*, 2025, **13**(37), 19212–19225, DOI: 10.1039/D5TC01938A.

6 J. E. Greiner, A. Singh and M. I. S. Röhr, Functionality Optimization for Effective Singlet Fission Coupling Screening in the Full-Dimensional Molecular and Intermolecular Coordinate Space, *Phys. Chem. Chem. Phys.*, 2024, **26**(28), 19257–19265, DOI: 10.1039/D4CP01274G.

7 T. Okada, F. Wataru, K. Hiroshi and H. Matsui, Virtual Screening of N-Type Organic Semiconductors Using Exhaustive Band Structure Calculations, *Sci. Technol. Adv. Mater.:Methods*, 2025, **5**(1), 2442902, DOI: 10.1080/27660400.2024.2442902.

8 R. Gómez-Bombarelli, J. Aguilera-Iparraguirre, T. D. Hirzel, D. Duvenaud, D. Maclaurin, M. A. Blood-Forsythe, H. S. Chae, M. Einzinger, D. G. Ha, T. Wu, G. Markopoulos, S. Jeon, H. Kang, H. Miyazaki, M. Numata, S. Kim, W. Huang, S. I. Hong, M. Baldo, R. P. Adams and A. Aspuru-Guzik, Design of Efficient Molecular Organic Light-Emitting Diodes by a High-Throughput Virtual Screening and Experimental Approach, *Nat. Mater.*, 2016, **15**(10), 1120–1127, DOI: 10.1038/nmat4717.

9 C. F. Perkinson, D. P. Tabor, M. Einzinger, D. Sheberla, H. Utzat, T. A. Lin, D. N. Congreve, M. G. Bawendi, A. Aspuru-Guzik and M. A. Baldo, Discovery of Blue Singlet Exciton Fission Molecules *via* a High-Throughput Virtual Screening and Experimental Approach, *J. Chem. Phys.*, 2019, **151**(12), 121102, DOI: 10.1063/1.5114789.

10 A. Lunt, H. Fakhruldeen, G. Pizzuto, L. Longley, A. White, N. Rankin, R. Clowes, B. Alston, L. Gigli, G. M. Day, A. I. Cooper and S. Y. Chong, Modular, Multi-Robot Integration of Laboratories: An Autonomous Workflow for Solid-State Chemistry, *Chem. Sci.*, 2024, **15**(7), 2456–2463, DOI: 10.1039/D3SC06206F.

11 B. Burger, P. M. Maffettone, V. V. Gusev, C. M. Aitchison, Y. Bai, X. Wang, X. Li, B. M. Alston, B. Li, R. Clowes, N. Rankin, B. Harris, R. S. Sprick and A. I. Cooper, A Mobile Robotic Chemist, *Nature*, 2020, **583**(7815), 237–241, DOI: 10.1038/s41586-020-2442-2.

 © 2026 The Author(s). Published by the Royal Society of Chemistry

12 J. Terence Blaskovits, M. H. Garner and C. Corminboeuf, Symmetry-Induced Singlet-Triplet Inversions in Non-Alternant Hydrocarbons, *Angew. Chem.*, 2023, **135**(15), e202218156, DOI: 10.1002/ange.202218156.
13 Ö. H. Omar, X. Xie, A. Troisi and D. Padula, Identification of Unknown Inverted Singlet-Triplet Cores by High-Throughput Virtual Screening, *J. Am. Chem. Soc.*, 2023, **145**(36), 19790–19799, DOI: 10.1021/jacs.3c05452.
14 H. Wang, J. Wang, T. Zhang, Z. Xie, X. Zhang, H. Sun, Y. Xiao, T. Yu and W. Huang, Breaching Kasha's Rule for Dual Emission: Mechanisms, Materials and Applications, *J. Mater. Chem. C*, 2021, 10154–10172, DOI: 10.1039/d1tc01970h.
15 C. Si, T. Wang, Y. Xu, D. Lin, D. Sun and E. Zysman-Colman, A Temperature Sensor with a Wide Spectral Range Based on a Dual-Emissive TADF Dendrimer System, *Nat. Commun.*, 2024, **15**(1), 7439, DOI: 10.1038/s41467-024-51231-x.
16 R. Gui, H. Jin, X. Bu, Y. Fu, Z. Wang and Q. Liu, Recent Advances in Dual-Emission Ratiometric Fluorescence Probes for Chemo/Biosensing and Bioimaging of Biomarkers, *Coord. Chem. Rev.*, 2019, 82–103, DOI: 10.1016/j.ccr.2019.01.004.
17 C. Li, J. Liang, B. Liang, Z. Li, Z. Cheng, G. Yang and Y. Wang, An Organic Emitter Displaying Dual Emissions and Efficient Delayed Fluorescence White OLEDs, *Adv. Opt. Mater.*, 2019, **7**(10), 1801667, DOI: 10.1002/adom.201801667.
18 L. Hou, X. Zhang, G. F. Cotella, G. Carnicella, M. Herder, B. M. Schmidt, M. Pätzel, S. Hecht, F. Cacialli and P. Samorì, Optically Switchable Organic Light-Emitting Transistors, *Nat. Nanotechnol.*, 2019, **14**(4), 347–353, DOI: 10.1038/s41565-019-0370-9.
19 M. Kasha, Characterization of Electronic Transitions in Complex Molecules, *Discuss. Faraday Soc.*, 1950, 14–19, DOI: 10.1039/DF9500900014.
20 R. Englman and J. Jortner, The Energy Gap Law for Radiationless Transitions in Large Molecules, *Mol. Phys.*, 1970, **18**(2), 285–287, DOI: 10.1080/00268977000100171.
21 N. J. Turro, V. Ramamurthy and J. C. Scaiano, Modern Molecular Photochemistry of Organic Molecules, *Photochem. Photobiol.*, 2012, **88**(4), 1033, DOI: 10.1111/j.1751-1097.2012.01178.x.
22 B. H. Jhun, D. Y. Jeong, S. Nah, S. Y. Park and Y. You, Novel Anti-Kasha Fluorophores Exhibiting Dual Emission with Thermally Activated Delayed Fluorescence through Detouring Triplet Manifolds, *J. Mater. Chem. C*, 2021, **9**(22), 7083–7093, DOI: 10.1039/d1tc00660f.
23 A. P. Demchenko, V. I. Tomin and P. T. Chou, Breaking the Kasha Rule for More Efficient Photochemistry, *Chem. Rev.*, 2017, **117**(21), 13353–13381, DOI: 10.1021/acs.chemrev.7b00110.
24 M. Beer and H. C. Longuet-Higgins, Anomalous Light Emission of Azulene, *J. Chem. Phys.*, 1955, **23**(8), 1390–1391, DOI: 10.1063/1.1742314.
25 K. Veys and D. Escudero, Computational Protocol to Predict Anti-Kasha Emissions: The Case of Azulene Derivatives, *J. Phys. Chem. A*, 2020, **124**(36), 7228–7237, DOI: 10.1021/acs.jpca.0c05205.
26 A. Diaz-Andres, J. Marín-Beloqui, J. Wang, J. Liu, J. Casado and D. Casanova, Rational Design of Anti-Kasha Photoemission from a Biazulene Core Embedded in an Antiaromatic/Aromatic Hybrid, *Chem. Sci.*, 2023, **14**(23), 6420–6429, DOI: 10.1039/D3SC00405H.
27 Z. Xu, J. Owona, Q. T. Liu, S. Putwa, L. Jiang, K.-M. Tong, D. Hean, B. O. Patrick, K. C. Chou, C. Tonnelé, F. Castet, D. Casanova and M. O. Wolf, A New Class of Diarylethene Compounds That Exhibit Turn-On Emission: From Aggregation-Induced Emission to Anti-Kasha Emission, *Adv. Opt. Mater.*, 2025, 422, DOI: 10.1002/adom.202500422.
28 T. Itoh, Fluorescence and Phosphorescence from Higher Excited States of Organic Molecules, *Chem. Rev.*, 2012, 4541–4568, DOI: 10.1021/cr200166m.
29 N. A. Kukhta and M. R. Bryce, Dual Emission in Purely Organic Materials for Optoelectronic Applications, *Mater. Horiz.*, 2021, 33–55, DOI: 10.1039/d0mh01316a.
30 J. L. Belmonte-Vázquez, Y. A. Amador-Sánchez, L. A. Rodríguez-Cortés and B. Rodríguez-Molina, Dual-State Emission (DSE) in Organic Fluorophores: Design and Applications, *Chem. Mater.*, 2021, 7160–7184, DOI: 10.1021/acs.chemmater.1c02460.
31 F. Li, G. Jiang, M. Li, J. Fan, Y. Song, C.-K. Wang and L. Lin, Thermally Activated Delayed Fluorescence Emitters with Dual Conformations for White Organic Light-Emitting Diodes: Mechanism and Molecular Design, *Phys. Chem. Chem. Phys.*, 2020, **22**(3), 1313–1323, DOI: 10.1039/C9CP05552E.
32 M. Röhrs and D. Escudero, Multiple Anti-Kasha Emissions in Transition-Metal Complexes, *J. Phys. Chem. Lett.*, 2019, **10**(19), 5798–5804, DOI: 10.1021/acs.jpclett.9b02477.
33 S. Ladouceur, L. Donato, M. Romain, B. P. Mudraboyina, M. B. Johansen, J. A. Wisner and E. Zysman-Colman, A Rare Case of Dual Emission in a Neutral Heteroleptic Iridium(Iii) Complex, *Dalton Trans.*, 2013, **42**(24), 8838–8847, DOI: 10.1039/c3dt33115f.
34 D. Gormin and M. Kasha, Triple Fluorescence in Aminosalicylates. Modulation of Normal, Proton-Transfer, and Twisted Intramolecular Charge-Transfer (TICT) Fluorescence by Physical and Chemical Perturbations, *Chem. Phys. Lett.*, 1988, **153**(6), 574–576, DOI: 10.1016/0009-2614(88)85263-1.
35 I. Bhattacharjee, N. Acharya, H. Bhatia and D. Ray, Dual Emission through Thermally Activated Delayed Fluorescence and Room-Temperature Phosphorescence, and Their Thermal Enhancement *via* Solid-State Structural Change in a Carbazole-Quinoline Conjugate, *J. Phys. Chem. Lett.*, 2018, **9**(11), 2733–2738, DOI: 10.1021/acs.jpclett.8b00937.
36 C. Li, R. S. Nobuyasu, Y. Wang, F. B. Dias, Z. Ren, M. R. Bryce and S. Yan, Solution-Processable Thermally Activated Delayed Fluorescence White OLEDs Based on Dual-Emission Polymers with Tunable Emission Colors and Aggregation-Enhanced Emission Properties, *Adv. Opt. Mater.*, 2017, **5**(20), 1700435, DOI: 10.1002/adom.201700435.

© 2026 The Author(s). Published by the Royal Society of Chemistry

37 J. C. del Valle and J. Catalán, Kasha's Rule: A Reappraisal, *Phys. Chem. Chem. Phys.*, 2019, **21**(19), 10061–10069, DOI: 10.1039/C9CP00739C.
38 J. J. Irwin and B. K. Shoichet, ZINC - A Free Database of Commercially Available Compounds for Virtual Screening, *J. Chem. Inf. Model.*, 2005, **45**(1), 177–182, DOI: 10.1021/ci049714+.
39 D. Weininger, SMILES, a Chemical Language and Information System. 1. Introduction to Methodology and Encoding Rules, *J. Chem. Inf. Comput. Sci.*, 1988, **28**(1), 31–36, DOI: 10.1021/ci00057a005.
40 A. K. Rappe, C. J. Casewit, K. S. Colwell, W. A. Goddard and W. M. Skiff, UFF, a Full Periodic Table Force Field for Molecular Mechanics and Molecular Dynamics Simulations, *J. Am. Chem. Soc.*, 1992, **114**(25), 10024–10035, DOI: 10.1021/ja00051a040.
41 https://www.rdkit.org.
42 X. Wu, X. Xie and A. Troisi, Calibration of Several First Excited State Properties for Organic Molecules through Systematic Comparison of TDDFT with Experimental Spectra, *J. Mater. Chem. C*, 2024, **12**(46), 18886–18892, DOI: 10.1039/D4TC03511A.
43 M. A. Robb Conical Intersections in Organic Photochemistry, in *Conical Intersections: Theory, Computation and Experiment*, 2011, pp. 3–50, DOI: 10.1142/9789814313452_0001.
44 Y. Tu, Z. Zhao, J. W. Y. Lam and B. Z. Tang, Mechanistic Connotations of Restriction of Intramolecular Motions (RIM), *Natl. Sci. Rev.*, 2021, **8**(6), nwaa260, DOI: 10.1093/nsr/nwaa260.
45 Ö. H. Omar, X. Xie, A. Troisi and D. Padula, Identification of Unknown Inverted Singlet–Triplet Cores by High-Throughput Virtual Screening, *J. Am. Chem. Soc.*, 2023, **145**(36), 19790–19799, DOI: 10.1021/jacs.3c05452.
46 L. Barneschi, L. Rotondi and D. Padula, Molecular Geometry Impact on Deep Learning Predictions of Inverted Singlet–Triplet Gaps, *J. Phys. Chem. A*, 2024, **128**(12), 2417–2426, DOI: 10.1021/acs.jpca.4c00172.
47 A. Coxson, Ö. H. Omar, M. del Cueto and A. Troisi, Predicting S_1 TDDFT Energies from ZINDO Calculations Using Message-Passing ΔML with Electronically Informed Descriptors, *J. Chem. Theory Comput.*, 2026, **22**(3), 1476–1490, DOI: 10.1021/acs.jctc.5c01587.
48 W. Thorwart; U. Gebert; R. Schleyerbach and R. R. Bartlett.Substituted 3-Phenyl-7H-Thiazolo[3,2-b][1,2,4] Triazin-7-ones, *Processes for Their Preparation, Medicaments Containing Them and Their Use*, 1989.
49 M. Renoud-Grappin, C. Fossey, G. Fontaine, D. Ladurée, A. M. Aubertin and A. Kirn, Imidazo[1,5-b]Pyridazine-D4T Conjugates: Synthesis and Anti-Human Immunodeficiency Virus Evaluation, *Antiviral Chem. Chemother.*, 1998, **9**(3), 205–223, DOI: 10.1177/095632029800900302.
50 W. Song, Q. Xu, J. Zhu, Y. Chen, H. Mu, J. Huang and J. Su, Imidazo[1,2- b]Pyridazine as Building Blocks for Host Materials for High-Performance Red-Phosphorescent Organic Light-Emitting Devices, *ACS Appl. Mater. Interfaces*, 2020, **12**(17), 19701–19709, DOI: 10.1021/acsami.9b22060.
51 A. Tigreros, S. L. Aranzazu, N. F. Bravo, J. Zapata-Rivera and J. Portilla, Pyrazolo[1,5-: A] Pyrimidines-Based Fluorophores: A Comprehensive Theoretical-Experimental Study, *RSC Adv.*, 2020, **10**(65), 39542–39552, DOI: 10.1039/d0ra07716j.
52 D. Z. Hook, R. Kilbride, D. J. Gillard, S. M. Rivero, R. K. Venkatraman, J. P. Pidgeon, A. Tartakovskii and J. Clark, The Importance of Accounting for Non-Radiative Decay When Screening Materials for Singlet Fission: The Case of Pigment Red 254, *J. Mater. Chem. C*, 2025, **13**(33), 16981–16997, DOI: 10.1039/d5tc01336d.
53 T. Pizza, A. Troisi and A. Capobianco, Computation of Nonradiative Rates for High-Throughput Virtual Screening: Application to the Discovery of Potential TADF Molecules, *J. Chem. Theory Comput.*, 2026, **22**(17), 9100–9108, DOI: 10.1021/acs.jctc.6c00881.
54 T. Mariana, M. T. do Casal, K. Veys, M. H. E. Bousquet, D. Escudero and D. Jacquemin, First-Principles Calculations of Excited-State Decay Rate Constants in Organic Fluorophores, *J. Phys. Chem. A*, 2023, **127**, 10033–10053, DOI: 10.1021/acs.jpca.3c06191.

© 2026 The Author(s). Published by the Royal Society of Chemistry